Nanoscale

Accepted Manuscript

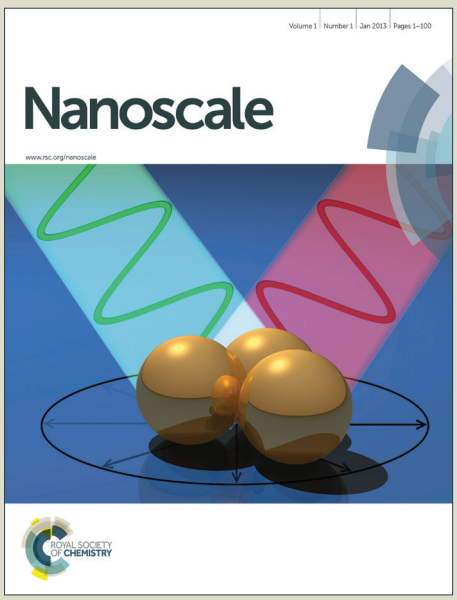

ROYAL SOCIETY OF CHEMISTRY

www.rsc.org/nanoscale

PdPt bimetallic nanoparticles enabled by shape control with halide ions and their enhanced catalytic activities

Jinfeng Zhang,[a] Lei Wan,[a] Lei Liu,[a] Yida Deng,*,[b] Cheng Zhong,[c] Wenbin Hu*,[a, b, c]

[a]State Key Laboratory of Metal Matrix Composites, Shanghai Jiao Tong University, Shanghai 200240, P. R. China

[b]Tianjin Key Laboratory of Composite and Functional Materials and [c]Key Laboratory of Advanced Ceramics and Machining Technology (Ministry of Education), Tianjin University, Tianjin 300072, P. R. China

*Email: yida.deng@tju.edu.cn; wbhu@263.net

Absract

In this work, a new and convenient approach in one step is described to synthesize shape controllable PdPt bimetallic nanoparticles. It is found that the resultant morphologies of these PdPt nanoparticles can be well controlled by just altering the participation of different halide ions serving as shape controlling agents in the reaction solution. The dendritic core-shell PdPt bimetallic nanoparticles generated with Pt atoms taking a usual island growth pattern in the presence of Cl^- ions, while the introduction of Br^- ions with relative strong adsorption effect would allow the formation of layered core-shell structure due to the layered growth mode of Pt atoms on the exterior surface of central Pd core. Moreover, the stronger adsorption function of I^- ions and the resulting fast atomic diffusion promoted the generation of mesoporous core-shell PdPt bimetallic nanoparticles with many pore channels. In addition, the size of these synthesized PdPt nanoparticles exhibited a significant dependence on the concentration of the halide ions involved. Due to their specific structural features and synergistic effects, they exhibited shape-dependent catalytic performance and drastically enhanced electrocatalytic activities relative to commercial Pt black and Pt/C for these PdPt catalysts toward methanol oxidation.

Introduction

It is well known that noble metal Pt is widely used as the effective catalyst owing to its superior catalytic activity for fuel cells.[1–5] However, considering the limited reserves and high cost of Pt, it is urgent to reduce the consumption of pure Pt used in the application, and it is also important to improve its poison resistance resulting from the strong adsorption of CO intermediates generated in the catalytic process which lower the activity and stability.[6–9] In addition, compared with monometallic nanoparticles, bimetallic ones exhibit enhanced catalytic performance resulting from their special structures and synergistic effect between the two elemental compositions.[10–12] Besides, owing to the same face centered cubic (fcc) structure and

the similar lattice constants with a mismatch of 0.77% of Pd and Pt, more abundant and less expensive Pd along with excellent performance in catalysis is the highly promising candidate to prepare bimetallic nanomaterials.[13–15] To these ends, bimetallic Pd based nanomaterials with the reduction of Pt content have attracted great interest for the past few years.[16, 17] Xia's group deposited Pt atoms as ultrathin skins of only a few atomic layers thick on the cubic Pd substrate for core-shell PdPt nanocubes which showed enhanced activity toward oxygen reduction attributed to the weakening OH binding energy through a combination of ligand and strain effects.[18] Taking advantage of precursor ligand effects, Skrabalak et al achieved core-shell and alloyed structure PdPt bimetallic nanomaterials via co-reduction.[19, 20] Huang reported that the obtained PdPt nanocrystals enclosed by specific facets with cubic, octahedral or tetrahedral morphologies showed high activities for hydrogenation of nitrobenzene.[21] In Yamauchi's work, the synthesized bimetallic nanodendrites with Pd core and Pt shell demonstrated superior catalytic performance in methanol oxidation.[22] Nevertheless, there are still limited reports on the preparation of bimetallic PdPt nanoparticles with favorable structures such as dendritic or porous morphologies with direct one-step synthetic method in aqueous-phase solution and the studies of their outstanding catalytic properties owing to not only the lower density and the greatly accessible surface area but also the synergistic effect of the two metals. Therefore, it is still a significant challenge to readily achieve these unique and desirable structures with shape tunability via a simple and direct synthetic strategy, as well as study their improved and shape-dependent catalytic activities related to nanostructures and synergistic effect.

As demonstrated in our previous work,[23] Pd nanoparticles with shape evolution from nanocubes to octahedrons were prepared through hydrochloric acid oxidative etching. The concentration of HCl was found to play a key role in the shape evolution. Moreover, to our knowledge, with the requirements of iodide ions as morphology controller and acetylacetonates as metal precursors, Zheng and his co-workers prepared hollow PdPt single-crystalline nanocubes.[24] It is noteworthy that these synthetic PdPt bimetallic nanoparticles[24–27] previously reported were usually prepared with the required conditions of either a multistep seed-mediated growth method producing Pd nanoparticles firstly served as the seeds, organic precursors, one specific kind of halide ions or a high reaction temperature for a long time, and their corresponding catalytic activities rarely studied up to now. In light of the above reasons and the understanding of the vital function for halides ions, PdPt bimetallic nanoparticles were synthesized by introducing different halide ions based on our previous method for the synthesis of Pd nanoparticles. Noticeably, compared to the previously reported approaches to prepare PdPt bimetallic nanoparticles, there are several highlights for our strategies: first, the distinct morphological PdPt bimetallic nanoparticles were prepared with both metal precursors present simultaneously in aqueous solution. It is quite different from the traditional seed-mediated method with premade Pd nanoparticles as seeds. Second, the PdPt bimetallic nanoparticles with various morphologies including dendritic core-shell, layered core-shell and mesoporous core-shell structures in high purity can be readily achieved only by

adding different halides with certain amounts to the reaction solution. Finally, this synthetic method with only altering the presence of different halides ions in the same reaction system which avoids the influencing induced by other factors from diverse reaction system, facilitating our understanding for the possible influencing mechanism of various halide ions served as shape controlling agents toward the shape of PdPt bimetallic nanoparticles. Moreover, the catalytic activities of these resultant PdPt nanoparticles were investigated. It was demonstrated that the obtained PdPt nanoparticles displayed shape-dependent enhanced catalytic activity and durability relative to that of commercial Pt black and Pt/C toward methanol oxidation. This work not only provides a simple and feasible approach in one step to the synthesis of PdPt bimetallic nanoparticles with desirable structures which facilitate the highly enhanced catalytic performance for methanol oxidation, but also advances our understanding for the function of various halide ions involved in the synthesis and may be a synthetic reference for the preparation of other bimetallic nanoparticles with desired morphologies and performances.

Results and discussion

The dendritic core-shell PdPt bimetallic nanoparticles with central Pd core and dendritic Pt exterior were synthesized in one-step method by introducing 80 mM NaCl to the mixture solution with Pd precursors and Pt precursors simultaneously present, as illustrated in Figure 1a. The nanoparticle size ranged narrowly from 39 nm to 47 nm, with an average size of 43 nm. It is found that Pd precursors got reduced before Pt ones. To visualize the different reduction rate of the two precursors, two vials with cetylpyridinium chloride (CPC) solution containing H_2PdCl_4 and H_2PtCl_6 respectively were prepared, as soon as the reduction agent ascorbic acid (AA) was injected into the two vials at 90 ℃, a rapid color change can be observed for Pd precursors solution, but almost unchanged for Pt ones (Figure S1). This observation is in good agreement with the result of preferential production of Pd cores for the synthesis of PdPt nanoparticles involving Pd precursors and Pt precursors at the same time, confirming the faster reduction rate of Pd precursors. Previous studies reported that[28] there were several Pt(IV) species due to the aqua and hydroxo substitution for $PtCl_6^{2-}$ complex in aqueous solution, which would affect the reduction kinetics of Pt(IV). The use of CPC aqueous solution may make it possible for the preferential reduction of Pd precursors than Pt ones. Thus, an instantaneous nucleation and growth of Pd occurred, and Pd-rich cores were formed followed by subsequent deposition of Pt atoms on the outer surface. Besides, it is known that Pt tends to deposit and grow in island mode due to the intrinsic high surface free energy and interatomic bond energy.[18, 29] Therefore, the later nucleation and deposition of Pt atoms in the pattern of island on central Pd cores surface finally generated the obvious PdPt dendritic core-shell structure.

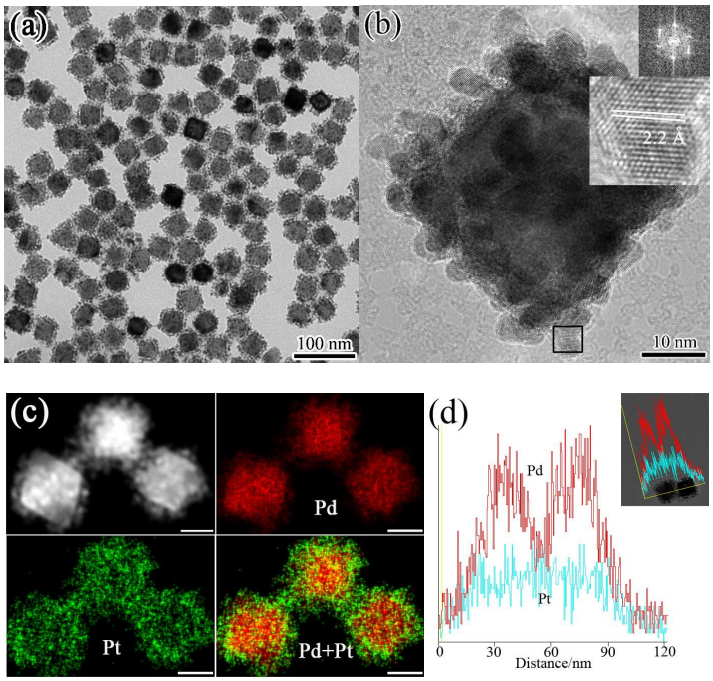

Figure 1. (a) TEM image, (b) HRTEM image, (c) HAADF-STEM image together with the corresponding EDX mapping (The scale bars are 20 nm.), and (d) Line scan profiles of dendritic core-shell PdPt bimetallic nanoparticles synthesized according to the standard procedure in the presence of 80 mM NaCl.

The HRTEM image of an individual dendritic PdPt nanoparticle shown in Figure 1b indicates that Pt branch with the epitaxial overgrowth on the outer surface of Pd nanoparticle is single crystalline structure, demonstrating the subsequently direct nucleation and growth of Pt on the preferentially formed central Pd core rather than self-nucleation to generate large particles. The corresponding Fourier transform (FT) pattern is also shown in the insets. The lattice spacing is about 2.2 Å, which corresponds to the {111} facets of fcc Pt.[16] It is noteworthy that the outer island Pt shell composed of many Pt nanoparticles in small size provided high surface area for all these dendritic core-shell PdPt nanoparticles. This structure is highly favorable for the enhancement of catalytic activity. Figure 1c shows the high-angle annular dark-field scanning transmission electron microscope (HAADF-STEM) image and the corresponding energy-disperse X-ray (EDX) mapping of dendritic PdPt bimetallic nanoparticles. As observed, the intense contrast between the core and the outer surface, indicating the dendritic core-shell morphology. Specifically, this discrete and dendritic structure can be more clearly seen in the EDX mapping, in which Pd nanoparticle is concentrated in the center, whereas some Pt nanoparticles in the form of island are distributed on the exterior surface. Additionally, the EDX line scan analysis across two PdPt bimetallic nanoparticles is shown in Figure 1d. Obviously, for a single PdPt nanoparticle, the peak of Pd element in the middle and the relatively flat trace of Pt element, this elemental distribution further confirms the dentritic core-shell structure of PdPt with core rich in Pd, while the entire surface layer coated by Pt branches. The wide-angle X-ray diffraction (XRD) profile for dendritic

core-shell PdPt indicates the fcc structure (Figure S2) of the obtained nanoparticles and it is difficult to distinguish Pd and Pt in the XRD pattern because of their extremely high lattice match. Beside, the composition analysis investigated by energy dispersive X-ray spectroscope (EDS) (Figure S3) and inductively coupled plasma-mass spectroscopy (ICP-MS) (Table S1) show that the Pt atomic percentage content is about 13.6 at.% for dendritic core-shell PdPt nanoparticles.

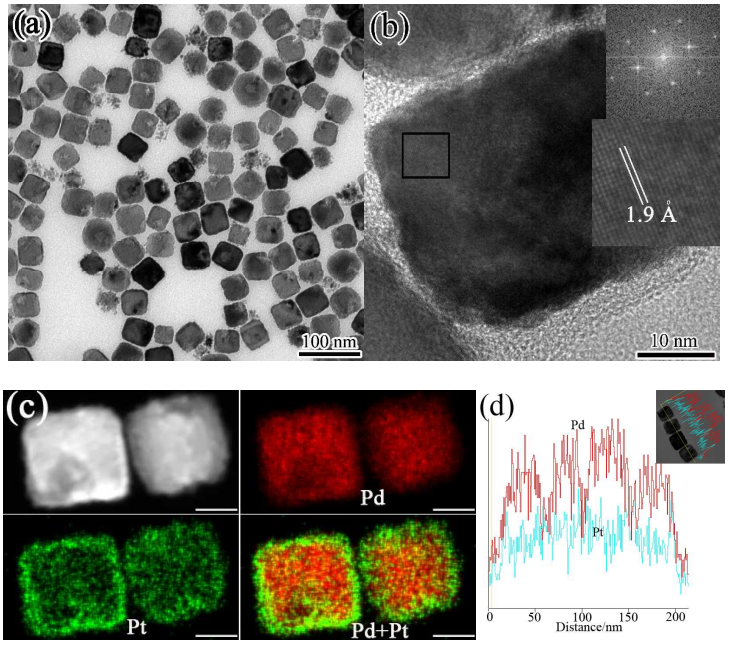

Figure 2. (a) TEM image, (b) HRTEM image, (c) HAADF-STEM image together with the corresponding EDX mapping (The scale bars are 20 nm.), and (d) Line scan profiles of layered core-shell PdPt bimetallic nanoparticles synthesized under the same conditions as the synthesis of dendritic core-shell PdPt bimetallic nanoparticles, except that 80 mM NaCl was replaced by 80 mM NaBr.

While NaCl in the reaction was substituted with NaBr at the same concentration, the obviously distinct shape of PdPt bimetallic nanoparticles was observed. As illustrated by TEM image in Figure 2a, the layered core-shell structure with an average size of 44 nm along with concave sites was formed. To investigate and validate the different reduction rate of Pd and Pt precursors in the presence of 80 mM NaBr, a set of experiments were conducted (Figure S4). Clearly, the results indicate the generation of Pd(II) and Pt(IV) bromide in the case of the addition of NaBr, which is reasonable due to the much larger stability constants of Pd(II) and Pt(IV) bromide than Pd(II) and Pt(IV) chloride.[25] Moreover, due to the difference of stability between Pd and Pt precursors, the faster nucleation of Pd than Pt occurred, which was also demonstrated by the rapid color change of Pd precursor solution reduced by AA. Therefore, most of Pt(IV) chloride transformed to Pt(IV) bromide in the presence of Br^- ions serving as the coordination ligand. In addition, because of the selective adsorption of Br^- ions on the Pd{100} facets, the formed Pt(IV) bromide mostly occupied the {100} facets of Pd nanocubes generated through the reduction of Pd precursors prior to Pt ones. As a result, by involving Br^- ions in the solution, the

atomic addition of Pt atoms would take place on the entire surface of Pd core, eventually lead to the formation of layered core-shell PdPt bimetallic nanoparticles with some excavated sites which result from the galvanic replacement reaction between Pd atoms and Pt precursors. As shown in Figure 2b, the fringes spacing of 1.9 Å marked on the surface of layered core-shell PdPt bimetallic nanoparticles synthesized with 80 mM NaBr, can be indexed to the {200} facets of fcc Pd or Pt. Due to the low lattice mismatch between Pd and Pt, it is difficult to distinguish the two elements from the lattice fringe spacing. The corresponding HAADF-STEM image and EDX mapping are shown in Figure 2c, indicating the layered core-shell structure of PdPt bimetallic nanoparticles with exterior layered Pt shells and central Pd core, as well as some excavated sites for Pd core and Pt shell demonstrating the occurrence of galvanic replacement between Pd atoms and Pt precursors. The EDX line scan profile (Figure 2d) further confirms the uniform distribution of Pt element for the whole surface of PdPt nanoparticle. The peak positions and intensities of the corresponding XRD pattern (Figure S2) also indicate the fcc structure for layered core-shell PdPt bimetallic nanoparticles. And the atomic percentage of Pt is 15.7 at.% according to ICP (Table S1) measurement which is comparable to the result of the EDS test (Figure S3).

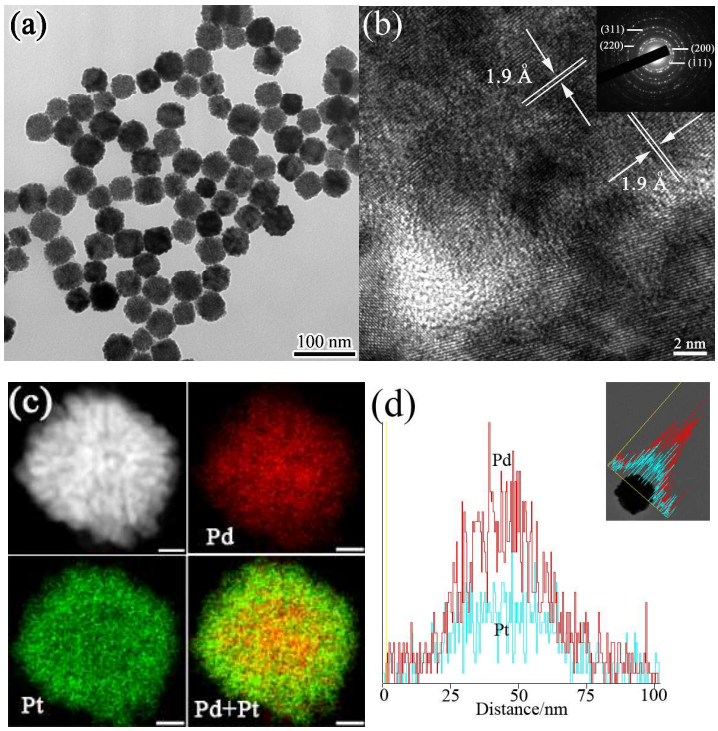

Figure 3. (a) TEM image, (b) HRTEM image, (c) HAADF-STEM image together with the corresponding EDX mapping (The scale bars are 10 nm.), and (d) Line scan profiles of mesoporous core-shell PdPt bimetallic nanoparticles synthesized under the same conditions as the synthesis of dendritic core-shell PdPt bimetallic nanoparticles, except that 80 mM NaCl was replaced by 80 mM NaI.

The halide I^- ions were also employed to investigate their effect to the morphology of yielded PdPt bimetallic nanoparticles. As Br^- ions were replaced by

the same concentration of I^- ions supplied by taking advantage of NaI in the solution, TEM image of the achieved mesoporous core-shell PdPt nanoparticles of approximate 46 nm in size is shown in Figure 3a. It was well known that the adsorption effect enabled by different halide ions adsorbed on the Pd facets generally decreased in the order $I^- > Br^- > Cl^-$.[30] As such, I^- ions are supposed to adsorb strongly on the surface of preferentially formed Pd cores. And similarly, I^- ions as the strong coordination ligand facilitate the production of Pd(II) and Pt(IV) iodide as dominating precursors which are consistent with the phenomenon during the controlled experiments, and Pd precursors are also readily reduced by AA relative to Pt ones (Figure S5). So, the core-shell structure with Pd core and Pt shell was achieved. Moreover, previous report pointed out that,[24] I^- ions could enhance surface diffusion of atoms compared with other halide ions. Therefore, under suitable concentration of I^- ions, the fast diffusion outwards of Pd atoms participating in substitution reaction caused the generation of mesoporous Pt structure with many pore channels which could be regarded as the transportation channels in the galvanic replacement between Pd core and Pt precursors. The HRTEM image (Figure 3b) as well as the corresponding SAED pattern (inset) and the XRD pattern (Figure S2), reveal that the obtained PdPt bimetallic nanoparticles are fcc polycrystalline structure enclosed by most of exposed {100} facets. The HAADF-STEM image and the corresponding EDX mapping of an individual mesoporous core-shell PdPt bimetallic nanoparticle are shown in Figure 3c. It can be clearly seen that the product is mesoporous core-shell structure with many pore channels, and Pd as well as Pt elements distribute uniformly across a single particle. In addition, this homogeneous distribution together with the atomic ratio of the two elements can be further confirmed from the EDX line scan analysis (Figure 3d), EDS (Figure S3) and ICP results (Table S1) with 32.9 at.% Pt content. Compared with the Pt content of PdPt bimetallic nanoparticles by employing Cl^- and Br^- ions, the more Pt content of mesoporous core-shell structure suggests that the galvanic replacement between Pd and Pt precursors seems to be facilitated by I^- ions.

Overall, PdPt bimetallic nanoparticles with distinct morphologies can be obtained by altering the addition of different halide ions. In order to further elucidate the effect of different halide ions on Pd core shape and the formation process of PdPt, a group of experiments was carried out (Figure S6 and Figure S7). Followed by the addition of AA for 1 min, the various shape of Pd nanoparticles can be observed. As to the situation for Cl^- ions, the resulting Pd particles about 40 nm in edge length were mostly cuboctahedrons. This results can be attributed to the excess H^+ and Cl^- ions introduced by the Pt precursors which resulted in the enhanced oxidative etching function to produce non-cubic Pd particles. And for Br^- ions, the obtained Pd particles were cubic shape and approximately sized 75 nm, which can be ascribed to the absorption effect of Br^- ions to protect the surface of Pd from etching. In brief, the difference in morphology and size for generated Pd are unsurprising and in accordance with our previous study for the shape evolution of single crystal Pd particles under the influence of Cl^- and Br^- ions.[23] In the case of I^- ions, amounts of small Pd particles aggregated to many 30 nm large particles. A possible explanation for this observation might be that the presence of I^- ions accelerated the reduction of

Pd precursors to generate much smaller Pd particles on one hand, and these small-sized Pd particles grew to large ones through aggregation to decrease surface energy on the other. As these reactions proceeded for 40 min, all these products grew large with average size of 61 nm, 106 nm and 59 nm for PdPt bimetallic nanopartilces in the presence of Cl^-, Br^-, and I^- ions, respectively. More importantly, the deposition of Pt on the surface of Pd exterior appeared, and the corresponding composition ratios were tested in EDS. Combined with the product sizes and elemental ratio after 6 h reaction time, it is noteworthy that the Pd core size first increased than decreased, which is rational due to the initially continued growth of Pd core and the subsequent consumption oxidized by Pt precursors in galvanic replacement reaction.

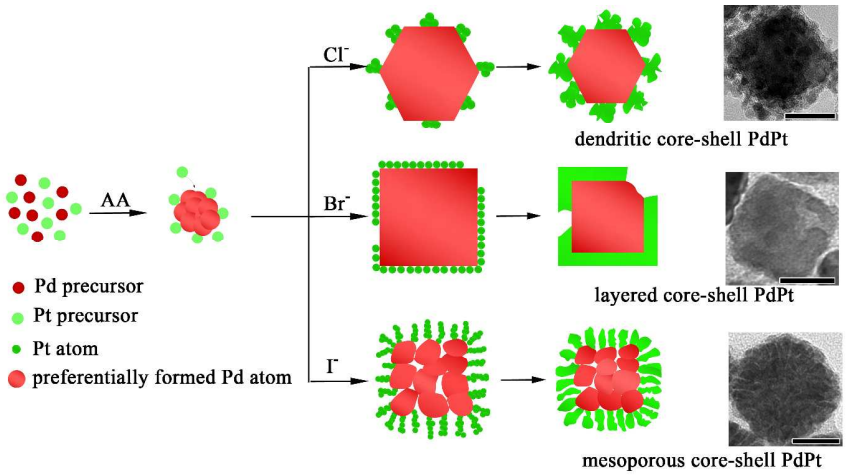

Figure 4. The schematic illustration of synthesized PdPt bimetallic nanoparticles with dendritic core-shell, layered core-shell, mesoporous core-shell structure by employing different halide ions with the same concentration of 80 mM and the corresponding TEM images (The scale bars are 20 nm.).

Based on all these results, Figure 4 illustrates the resultant core-shell structural PdPt bimetallic nanoparticles in different growth patterns of Pt on the central Pd core. Firstly, in this one-step synthetic method, it is found that no matter what kind of halide ions (Cl^-, Br^-, I^-) added, Pd was preferentially nucleated as central core upon reduction by AA. As previously mentioned, due to the high surface free energy and interatomic bond energy, Pt atoms had the tendency to deposit and grow in island mode. When moderate Cl^- ions with weak adsorption were introduced, the resulting reaction condition was still too mild to change the growth mode of Pt atoms. As a result, the still fast formation and deposition of Pt atoms facilitated Pt atoms to nucleate and grow in island pattern on the surface of newly formed Pd cores, PdPt bimetals with dendritic core-shell structure finally generated. While the synthesis was conducted by adding Br^- ions to substitute Cl^- ions, the adsorbed Br^- ions together with induced Pt(IV) bromide mostly covering the {100} facets of Pd caused a relatively slow generation rate of Pt atoms as well as the deposition onto the approximately entire surface of cubic Pd core. Consequently, the subsequent nucleation and epitaxial overgrowth of Pt atoms in layered pattern rather than island one on central Pd surface eventually produced layered core-shell PdPt bimetallic

nanoparticles. Here, the concave sites with exposed Pd exterior surface were supposed to result from the galvanic replacement of Pd atoms and Pt precursors and serve as transportation channel. Furthermore, if I^- ions with stronger adsorption than Br^- ions were used, on one hand, the coverage of the dominating Pt(IV) iodide on the Pd{100} would be beneficial to the uniform deposition of Pt atoms on the outer surface of collective Pd particles, on the other hand, the accelerated atomic diffusion function enhanced by I^- ions would promoted the formation of channels which favored Pd atoms to diffuse outwards to react with Pt precursors. Finally, mesoporous core-shell structure with amounts of chainlike path on the exterior Pt shell for PdPt bimetallic nanoparticles was obtained.

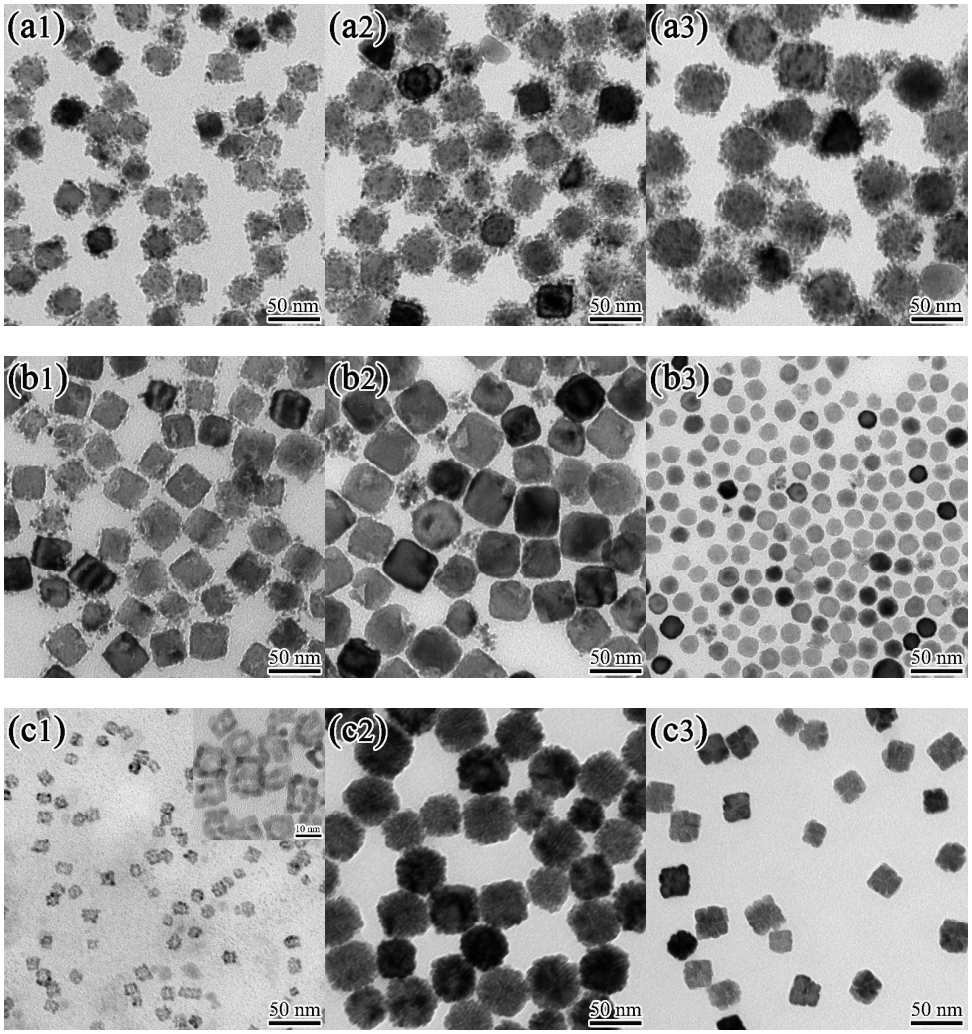

Figure 5. TEM images of PdPt bimetallic nanoparticles with distinct structures synthesized in the presence of various halides with different concentrations: (a1−a3) dendritic structure with NaCl in the concentration of 40 mM (a1), 80 mM (a2), 160 mM (a3); (b1−b3) layered structure with NaBr in the concentration of 40 mM (b1), 80 mM (b2), 160 mM (b3); (c1−c3) mesoporous structure with NaI in the concentration of 40 mM (c1), 80 mM (c2), 160 mM (c3).

The size of the resulting PdPt bimetallic nanoparticles can also be adjusted by changing the amount of halide ions involved. From the TEM images in Figure 5a1−a3,

with the increasing concentration of NaCl from 40 mM to 160 mM, the size of central Pd cores gradually increased. The size-dependent Pd cores are presumably due to the increasing addition of Cl^- ions slowing the reduction rate of Pd precursors and leading to the generation of fewer Pd nuclei and subsequent growth of larger Pd cores.

Figure 5b1−b3 shows the size controllable PdPt bimetallic nanoparticles with layered core-shell structure. Herein, Br^- ions play two key roles: first, Pt(IV) bromide generated by employing Br^- ions mainly cover the {100} facets of cubic Pd and the blocking effect of Br^- ions promote the layered growth of Pt on the surface of Pd cores. Second, the selective adsorption of Br^- ions on the Pd{100} facets would lower the reduction rate of Pd precursors to produce fewer Pd nuclei and the resulting increased size of central Pd cores. Therefore, with less Br^- ions in the concentration of 40 mM (Figure 5b1), the central Pd cores were apparently smaller than that of 80 mM Br^- ions (Figure 5b2). Besides, it should be noted that there are a small amount of island Pt nanoparticles in the outer surface of these layered PdPt bimetallic nanoparticles. This results may be accounted for the insufficient Br^- ions capping the newly formed layered Pt surface, thus causing a relatively fast Pt atomic deposition in island mode onto the Pt surface, which is similar to the grow mode of dendritic PdPt nanoparticles in the presence of Cl^- ions. In the presence of 80 mM Br^- ions, the small Pt branches on the external surface of PdPt bimetallic nanoparticles gradually decrease even disappear in comparison with the ones in Figure 5b1. Instead, a few aggregated Pt nanoparticles appeared, showing spontaneous separation apart from the layered PdPt bimetallic nanoparticles. These observations are presumably due to the fact that the sufficient Br^- ions with strong adsorption effect cap the surface of PdPt nanoparticles and slow the deposition rate of Pt atoms, thus avoiding the island growth of Pt atoms on the layered PdPt surface. On the other, a small amount of Pt atoms get together to form large nanoparticles via self-nucleation and random aggregation in the solution. If a further increase of Br^- ions concentration with 160 mM was performed, a decrease for the size of PdPt nanoparticles occurred, as shown in Figure 5b3. Taking Pt(IV) bromide $PtBr_6^{2-}$ an example, the reaction equation should take place under the condition of excessive Br^- ions in the solution:

$$2Pd + PtBr_6^{2-} + 2Br^- \rightarrow Pt + 2PdBr_4^{2-}$$

According to the equation above, the presence of excessive Br^- ions could promote the equilibrium to the right side. Furthermore, the molar volume of Pd and Pt is about 9 $cm^3\ mol^{-1}$.[8] Base on the molar ratio of Pd to Pt being 2:1, as a result, the ultimate PdPt bimetallic nanoparticles with decreased size were formed. Interestingly, the sharp corners of the small PdPt nanoparticles weakened even disappeared compared with previously as-obtained ones with low concentration of Br^- ions. A possible explanation might be the oxidative etching effect of Br^-/O_2 to some extent, which has been demonstrated in previous studies.[25, 31] This corrosion function initially dissolve the corners and edges of PdPt nanoparticles. Hence, the excessive Br^- ions favor the formation of these PdPt bimetallic nanoparticles with small size and nearly spherical profile. Additionally, according to the corresponding EDS (Figure S8c) results of these small PdPt nanoparticles, the increased content of Pt from EDS is also an indication that the excess Br^- ions promote the galvanic replacement reaction. In

order to further characterize the structure of this PdPt nanopaticles, the EDX line scan (Figure S8a) were performed, which shows not obviously core-shell structure, but the nearly mixed distribution of Pd and Pt for PdPt nanoparticles. The intensive galvanic replacement of Pd and Pt precursors with the assistant of excess Br^- ions should be responsible for the penetration of Pt atoms toward Pd core, and in view of this, this morphology was defined as mixed PdPt bimetallic structure.

Remarkably, in the case of a high concentration of 80 mM I^- ions, the apparent feature is the mesoporous Pt with pore channels on the central Pd core for PdPt nanoparticles with larger size (Figure 5c2). However, if 40 mM NaI were introduced in the synthesis of PdPt bimetallic nanoparticles, the structure with apparently hollow interiors and small size were formed, as shown in Figure 5c1. It is worth mentioning that this structure similar to nanoframe reported for other metals, [32, 33] have aroused our interest and would be further investigated in later research work. In the case of 80 mM I^- ions, the still existing solid Pd interior could be ascribed to the outcome of the initial larger Pd core caused by enough I^- ions greatly slowing down the reduction rate of Pd precursors. In subsequent galvanic replacement reaction, the larger Pd core fails to be consumed largely. Likewise, with 160 mM I^- ions present in aqueous solution (Figure 5c3), the subsequently decreased size of mesoporous structure could be explained with the mechanism similar to the case of 160 mM Br^- ions. That is, the excessive I^- ions promote the proceeding of the galvanic replacement between Pd and Pt(IV) iodide. Consequently, the total volume of the products decrease and the atomic ratio of Pt/Pd is close to 3 according to the results of EDS (Figure S8d) for this structure. Similarly, its corresponding EDX line scan (Figure S8b) for this structure was tested. It is found that the mixed structure with Pd and Pt elements is more obvious than that of PdPt nanoparticles in the presence of 160 mM Br^- ions.

In addition, when Cl^- ions were introduced by using HCl with different concentrations, the similar dendritic core-shell structure but different size for PdPt bimetallic nanoparticles can be achieved. When 40 mM NaCl was replaced by the same concentration of HCl, the central Pd cores with relatively large size generated, which was attributed to the slower reduction rate resulted from the use of acid HCl in the early nucleation stage (Figure 6a1). However, upon an increase of HCl, the resultant PdPt bimetallic nanoparticles turned into small ones, as illustrated in Figure 6a2. In this case, the nucleation rate was further reduced while introducing more amounts of HCl, but the oxidative etching of Cl^-/O_2 pair in acid condition was enhanced to preferentially dissolve new formed Pd from the corners of Pd particles in subsequent nuclei growth process, finally resulted in the production of Pd cores without sharp edges and the smaller size of PdPt bimetallic nanoparticles. In addition, the higher atomic percentage 18.07 at. % of Pt than that of one for PdPt under the condition of 80 mM NaCl from the corresponding ICP results (Table S1) further demonstrating the oxidative etching of Cl^-/O_2 pair enhanced by H^+ is beneficial to the occurrence of galvanic replacement. In the case of involving 160 mM HCl, the roughly equal size of central Pd core can be obtained compared to the one with 80 mM HCl, and the corresponding TEM image was shown in Figure 6a3. This result suggests that the shrinking size of Pd cores as a result of the oxidative etching

function fails to offset the substantially slowed reduction rate caused by the enlargement of Pd nucleus in the presence of excess HCl. However, the size of the outer Pt branches was slightly larger than the one prepared by using 80 mM HCl, which can be further confirmed by the compositional distribution of both Pd and Pt from the EDX line scan profiles in Figure 6b and c. The larger content of Pt (Figure 6c) might be ascribed to the excessive Cl^- ions which promote the galvanic replacement between Pd and $PtCl_6^{2-}$ to produce more Pt atoms. Taken together, the overall size of the resultant core-shell PdPt bimetallic nanoparticles could be effectively tuned simply by controlling the amount of halide ions from different additives in the solution.

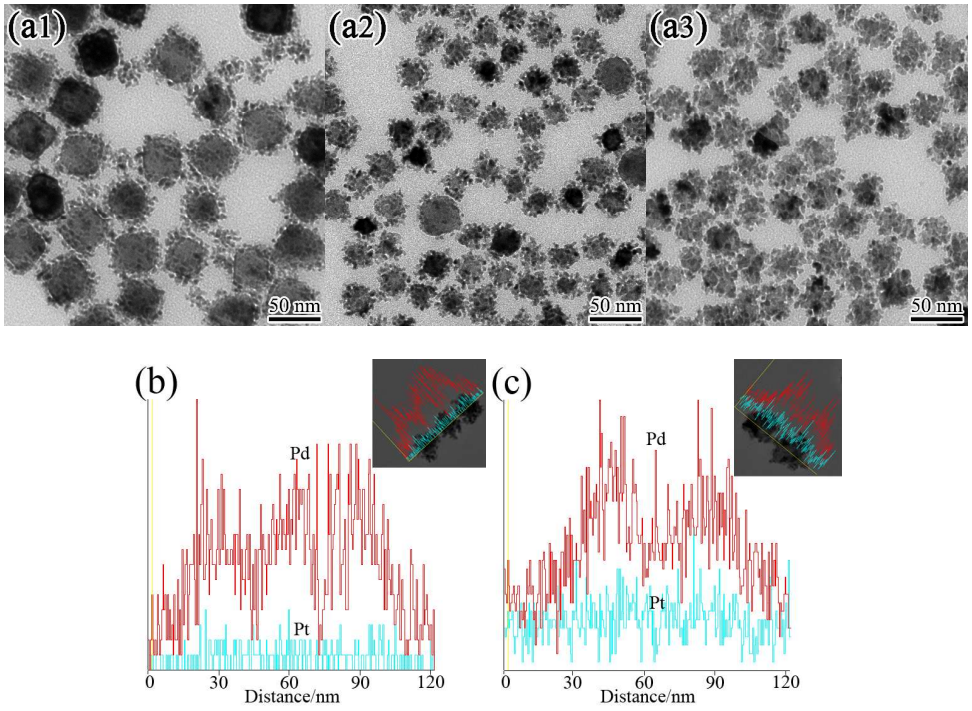

Figure 6. TEM images (a1−a3) of dendritic core-shell PdPt bimetallic nanoparticles synthesized according to the standard procedure, except that NaCl was replaced by HCl with the concentrations of 40 mM (a1), 80 mM (a2), 160 mM (a3), respectively. (b−c) Line scan profiles recorded from dendritic core-shell PdPt bimetallic nanoparticles corresponding to Figure 6a2, a3, respectively.

The synthesis of PdPt bimetallic nanoparticles without the involvement of any extra halide ions in one-step method was also conducted (Figure S9a). And the synthesized PdPt nanoparticles were also dendritic core-shell structure similar to the one by introducing Cl^- ions. For two-step method, that is to prepare Pd nanocubes in advance as seeds according to our previously reported method, followed by the addition of halides and Pt precursors in the mixture solution. When two-step seed-mediated approach with Pd nanocubes premade as seeds was taken, in the absence of halide, analogous morphology of dendritic core-shell PdPt bimetallic nanoparticles can be observed (Figure S9b). Taken together, this is also a confirmation that the Pt atoms deposit later on the Pd cores upon the preferential

reduction of Pd precursors in one-step method with two metal salts of Pd and Pt simultaneously present in the solution. However, a little difference can also be observed. The middle Pd cores of one-step method are larger in contrast to that of seed-mediated method. A possible explanation might be the reason that Cl^- ions released from Pt precursors increase the concentration of Cl^- ions in the solution with Pd precursors and Pt precursors simultaneously present, which lower the reduction rate at the initial nucleation stage, eventually result in the larger central Pd cores. In addition, in two-step method, the subsequent Pt atoms are mainly achieved by galvanic replacement between Pd atoms and Pt precursors, which consume central Pd cores and make their size decrease and morphology irregular. Moreover, PdPt bimetallic nanoparticles with similar dendritic core-shell, layered core-shell and mesoporous core-shell structures but smaller size can also be observed by involving different halides later for seed-mediated synthetic method (Figure S10). These results further imply that, for one-step approach, the halides not only cause the slow nucleation and the production of larger Pd nanoparticles as central cores, but also play a role in the subsequent growth mode of Pt atoms on the surface of cubic Pd cores owing to the adsorption effect of different halides.

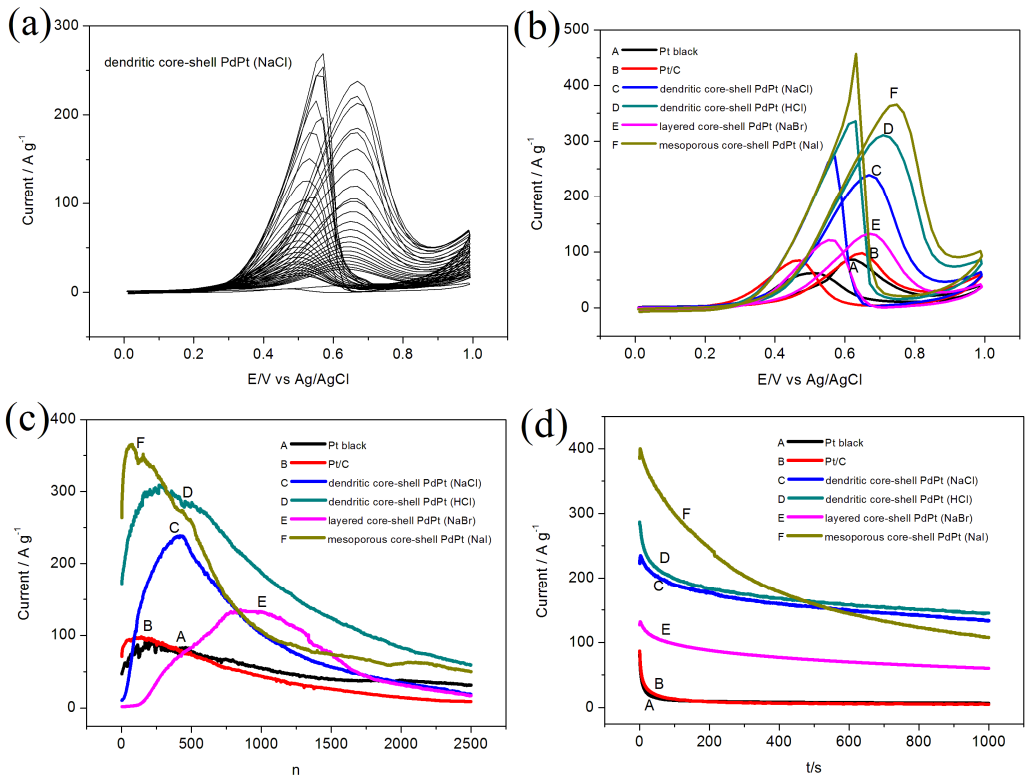

Figure 7. (a) CV curves of dendritic core-shell PdPt bimetallic nanoparticles in the presence of 80 mM NaCl from first to 2500th cycle in the solution of 0.1 M $HClO_4$ + 1 M CH_3OH at a scan rate of 50 $mV.s^{-1}$; (b) CV curves, (c) changes of peak current with increasing circle number, and (d) chronoamperometry curves at 0.67 V of commercial Pt black (A), commercial Pt/C (B), the obtained dendritic core-shell (C, D), layered core-shell (E) and mesoporous core-shell (F) PdPt bimetallic nanoparticles synthesized by involving 80 mM NaCl, HCl, NaBr and NaI, respectively measured in the solution of 0.1 M $HClO_4$ + 1 M CH_3OH at a scan rate of 50 $mV.s^{-1}$.

To measure the electrochemically active surface area (ECSA) of different PdPt bimetallic nanoparticles, cyclic voltammograms (CVs) were carried out in 0.1 M $HClO_4$ solution, and their corresponding specific ECSAs were calculated (Figure S11). For layered core-shell structure, the specific ECSA was 52.6 $m^2\ g_{Pt}^{-1}$, which is comparable to that of Pt/C (20 wt.% Pt, 53.7 $m^2\ g_{Pt}^{-1}$). The specific ECSA values for dendritic core-shell PdPt bimetallic nanoparticles were estimated to be 62.8 $m^2\ g_{Pt}^{-1}$ and 67.3 $m^2\ g_{Pt}^{-1}$ by employing 80 mM NaCl and 80 mM HCl, respectively. The slight higher value of specific ECSAs than that of Pt/C, especially for the ones using 80 mM HCl, may owe to the smaller size of PdPt and the island distribution of many small Pt particles outside the Pd core. For mesoporous core-shell PdPt, the favorable porous structure but relative large size, the two aspects might make the specific ECSA of 62.9 $m^2\ g_{Pt}^{-1}$ which is not too high. The large specific ECSAs of these PdPt nanoparticles suggest an promising application in catalysis.

The electrocatalytic activities of the prepared PdPt bimetallic nanoparticles toward methanol oxidation were investigated in the mixture solution containing 0.1 M $HClO_4$ and 1 M CH_3OH, and compared with commercial Pt black and Pt/C catalysts. Figure 7a shows CV curves of dendritic core-shell PdPt bimetallic nanoparticles synthesized by using 80 mM NaCl with increasing cycle number from beginning to 2500th cycle. The corresponding change of forward peak current is red plot (marked with B) shown in Figure 7c. It can be seen that the peak current increases evidently before the 400th cycle and then reach the maximum value. The catalytic performances of these PdPt bimetallic nanoparticles with various shapes are shown in Figure 7b and Figure S12. Obviously, the PdPt nanoparticles with mesoporous core-shell feature using NaI display the maximum peak current 366 A g_{Pd+Pt}^{-1}, higher than those of other morphologies and commercial Pt/C (98 A g_{Pt+C}^{-1}). The activity is about 3.7 times as active as the commercial Pt/C toward methanol oxidation. This outstanding performance can be attributed to the synergistic effect of Pd and Pt, and the special mesoporous core-shell structure which provides a large surface area and convenient channel to facilitate the fast transport of active species. Next, the dendritic core-shell PdPt nanoparticles also show superior catalytic activities. Moreover, the obtained ones employing 80 mM HCl demonstrate higher catalytic activities of 311 A g_{Pd+Pt}^{-1} than those of 239 A g_{Pd+Pt}^{-1} using 80 mM NaCl, due to the smaller size and slightly more Pt content for the former. With the addition of 80 mM NaBr, the achieved layered core-shell PdPt structure displaying more outstanding performance with 133 A g_{Pd+Pt}^{-1} than Pt/C catalyst is also observed. Meanwhile, it should be noted that the mass specific activity of dendritic core-shell PdPt for NaCl is 1.8 times as active as that of layered core-shell one with Pt weight percentage content of 22.45 wt.% for the former and 25.45 wt.% for the latter. This observation signifies that the nanostructures would remarkably affect the performance of methanol oxidation compared to the content of Pt.

Figure 7c shows the change trend of the catalytic activities for these distinct PdPt bimetallic nanoparticles with increasing cycle number. For all the samples, the peak currents gradually increase first, then decrease. The initial ascending process are supposed to be the activation stage of some active sites for various PdPt catalysts due

to their exposed surface apt to adsorb impurities. It is obvious that mesoporous core-shell PdPt catalysts with large surface area, especially for the porous structure across many small Pd and Pt particles, providing many active sites prone to activation reach the maximum peak current just through the fewest cycle number among all these catalysts, and layered core-shell PdPt ones with relatively tight surface relatively difficult to activate are the latest for reaching the maximum value. These observations are in good agreement with the morphologies of these PdPt bimetallic nanoparticles. It is also noticeable that the slower initial ascending and following descending of the catalytic activity. The stability of these PdPt nanoparticles were also been evaluated by chronoamperometry, and the results are illustrated in Figure 7d. It is found that the mesoporous core-shell ones exhibit a faster current decay with time in comparison with other catalysts, though its largest peak current among others which is consistent with the observation in Figure 7c. With the increase of catalytic cycle numbers, these exposed active sites would lost their activities more easily than that of dendritic and layered core-shell structure due to the accessible intermediate through the porous channels, thus the activity and stability would decline faster for mesoporous structure. The dendritic core-shell PdPt catalysts not only display enhanced activities but also good stability for methanol oxidation. Therefore, from all these results, the catalytic properties of these PdPt catalysts have a strong dependence on the structure related to the synergistic effect, which can be used as a reference of the structural design of different catalysts for catalytic application.

Conclusion

In summary, a simple one-step method for the synthesis of PdPt bimetallic nanoparticles has been developed. The key for the various shapes is the critical role of different halides serving as morphology controller in the preparation, which could induce the formation of distinct PdPt bimetallic nanoparticles with a variety of shapes, including dendritic core-shell, layered core-shell and mesoporous core-shell structures. Additionally, the size of these PdPt bimetallic nanoparticles can also be adjusted by changing the concentration of these halide ions added. The obtained different morphological PdPt catalysts exhibited dramatically enhanced catalytic activities compared to commercial Pt black for methanol oxidation, demonstrating their shape-dependent catalytic activities and promising potential as effective catalysts. Specifically, among these PdPt bimetallic nanoparticles, due to the large surface area and many pore channels of the ones with mesoporous core-shell structure showed the best activities. And the dendritic core-shell PdPt catalysts displayed both the improved catalytic performance and the durability. This work provides a simple and feasible route to prepare PdPt even other bimetallic nanoparticles with superior catalytic activities.

Experimental

Chemicals. Cetylpyridinium chloride (CPC, $C_{21}H_{38}ClN \cdot H_2O$, ≥99.0%), palladium chloride ($PdCl_2$, analytical grade), hexachloroplatinic acid ($H_2PtCl_6 \cdot 6H_2O$, analytical grade), hydrochloric acid (HCl, analytical grade), sodium chloride (NaCl, ≥99.0%),

sodium bromide (NaBr, ≥99.0%), sodium iodide (NaI, ≥99.0%), ascorbic acid (AA, $C_6H_8O_6$, ≥99.7%). All reagents were purchased from Sinopharm Chemical Reagent Co., Ltd and were used without further purification. The deionized water (18.2 MΩ·cm) used was prepared using an ultrapure water system (Millipore).

Synthesis of dendritic core-shell PdPt bimetallic nanoparticles. To prepare typical dendritic core-shell PdPt bimetallic nanoparticles, 10 mL of aqueous solution containing 20 mM CPC and 2 mL of 10 mM H_2PdCl_4 aqueous solution were mixed together in a glass vial. Next, 1 mL of NaCl with different concentrations (40 mM, 80 mM, 160 mM) was added into the mixture solution with stirring. Subsequently, 1 mL of 10 mM $H_2PtCl_6 \cdot 6H_2O$ aqueous solution was added. After the addition, the mixture was placed in water bath at 90 ℃ under magnetic stirring, followed by the quickly injection of 1 mL of 20 mM fresh reducing agent AA. The reaction was allowed to continue at 90 ℃ for 6 h. The size of dendritic core-shell PdPt nanoparticles can be adjusted by varying the amounts of NaCl. The products were collected via centrifugation and further purified with water and ethanol for several times.

Synthesis of layered core-shell and mesoporous core-shell PdPt bimetallic nanoparticles. The synthetic method for the preparation of layered core-shell PdPt bimetallic nanoparticles was similar to that of ones with dendritic core-shell structure except for substituting NaCl with NaBr into the reaction solution. Likewise, mesoporous core-shell PdPt nanoparticles can be obtained by replacing NaCl with NaI.

Characterizations. The morphologies and quantitative element analyses of the as-obtained PdPt bimetallic samples were characterized by transmission electron microscope (TEM), energy dispersive X-ray (EDX) line scanning and energy dispersive X-ray spectroscope (EDS) using a JEOL JEM-2100F field-emission electron microscope operated at 200 kV, and high resolution TEM (HRTEM), high-angle annular dark-field scanning TEM (HAADF-STEM), EDX mapping using FEI Talos operated at 200 kV. The percentages of Pd and Pt for PdPt catalysts in each sample were determined using inductively coupled plasma-mass spectroscopy (ICP-MS, 7500a). The structure of prepared PdPt was investigated by X-ray diffraction (XRD) patterns, which were obtained on a Rigaku Smartlab diffractometer with a Cu Kα radiation source (λ = 0.15406 nm).

Electrochemical measurements. Cyclic voltammograms (CVs) and chronoamperometry measurements were carried out on a CHI 660E electrochemical workstation using a conventional three-electrode cell. 15 μL of aqueous suspension of PdPt catalysts was dropped onto a glassy carbon electrode (GCE, 5 mm in diameter) as working electrode. A Pt foil and a Ag/AgCl (3.5 M KCl) were used as the counter and reference electrode, respectively. Then, the working electrode was covered with 8 μL of Nafion solution (0.2 wt %) and dried before electrochemical measurements. For measuring the electrochemically active surface area (ECSA), CVs were performed in N_2-purged 0.1 M $HClO_4$ solution at a sweep rate of 50 $mV.s^{-1}$, and then the specific ECSA was calculated. For methanol oxidation, the CVs and chronoamperometry curves were performed at a scan rate of 50 $mV.s^{-1}$ in a mixture solution of 0.1 M $HClO_4$ and 1 M CH_3OH solution.

Acnowledgements

This work was supported by the National Science Fund for Distinguished Young Scholars (No. 51125016) and the National Natural Science Foundation of China (No. 51571151).

Notes and references

1 S. Guo, S. Zhang, S. Sun, *Angew. Chem. Int. Ed.,* 2013, **52**, 8526.
2 D. Strmcnik, K. Kodama, D. Van der Vliet, J. Greeley, V. R. Stamenkovic, N. M. Marković, *Nat. Chem.,* 2009, **1**, 466.
3 M. Nakamura, R. Imai, N. Otsuka, N. Hoshi, O. Sakata, *J. Phys. Chem. C,* 2013, **117**, 18139.
4 M. Jin, H. Zhang, Z. Xie, Y. Xia, *Angew. Chem. Int. Ed.,* 2011, **50**, 7850.
5 X. Wang, Y. Orikasa, Y. Takesue, H. Inoue, M. Nakamura, T. Minato, N. Hoshi, Y. Uchimoto, *J. Am. Chem. Soc.,* 2013, **135**, 5938.
6 B. Y. Xia, H. B. Wu, X. Wang, X. W. Lou, *J. Am. Chem. Soc.,* 2012, **134**, 13934.
7 I. E. L. Stephens, I. Chorkendorff, *Angew. Chem. Int. Ed.,* 2011, **50**, 1476.
8 H. W. Liang, S. Liu, J. Y. Gong, S. B. Wang, L. Wang, S. H. Yu, *Adv. Mater.,* 2009, **21**, 1850.
9 Z. Chen, M. Waje, W. Li, Y. Yan, *Angew. Chem. Int. Ed.,* 2007, **46**, 4060.
10 J. Wu, L. Qi, H. You, A. Gross, J. Li, H. Yang, *J. Am. Chem. Soc.,* 2012, **134**, 11880.
11 B. Lim, M. Jiang, P. H. C. Camargo, E. C. Cho, J. Tao, X. Lu, Y. Zhu, Y. Xia, *Science,* 2009, **324**, 1302.
12 Y. Wu, D. Wang, Z. Niu, P. Chen, G. Zhou, Y. Li, *Angew. Chem. Int. Ed.,* 2012, **51**, 12524.
13 S. Li, J. Lv, L. Teng, A. Wang, J. Chen, J. Feng, *ACS Appl. Mater. Interfaces,* 2014, **6**, 10549.
14 H. Zhang, M. Jin, Y. Xia, *Chem. Soc. Rev.,* 2012, **41**, 8035.
15 A. Wang, H. Xu, J. Feng, L. Ding, Y. Tong, G. Li, *J. Am. Chem. Soc.,* 2013, **135**, 10703.
16 J. W. Hong, S. W. Kang, B. S. Choi, D. Kim, S. B. Lee, S. W. Han, *ACS Nano,* 2012, **6**, 2410.
17 Y. Liu, M. Chi, V. Mazumder, K. L. More, S. Sole, J. Henao, S. Sun, *Chem. Mater.,* 2011, **23**, 4199.
18 S. Xie, S, -I. Choi, N. Lu, L. T. Roling, J. A. Herron, L. Zhang, J. Park, J. Wang, M. J. Kim, Z. Xie, M. Mavrikakis, Y. Xia, *Nano Lett.,* 2014, **14**, 3570.
19 N. Ortiz, R. G. Weiner, S. E. Skrabalak, *ACS Nano,* 2014, **8**, 12461.
20 N. Ortiz, S. E. Skrabalak, *Angew. Chem. Int. Ed.,* 2012, **51**, 11757.
21 X. Huang, Y. Li, Y. Li, H. Zhou, X. Duan, Y. Huang, *Nano Lett.,* 2012, **12**, 4265.
22 L. Wang, Y. Nemoto, Y. Yamauchi, *J. Am. Chem. Soc.,* 2011, **133**, 9674.
23 J. Zhang, C. Feng, Y. Deng, L. Liu, Y. Wu, B. Shen, C. Zhong, W. Hu, *Chem. Mater.,* 2014, **26**, 1213.

24 X. Huang, H. Zhang, C. Guo, Z. Zhou, N. Zheng, *Angew. Chem.,* 2009, **121**, 4902.
25 H. Zhang, M. Jin, J. Wang, W. Li, P. H. C. Camargo, M. J. Kim, D. Yang, Z. Xie, Y. Xia, *J. Am. Chem. Soc.,* 2011, **133**, 6078.
26 H. Zhang, M. Jin, H. Liu, J. Wang, M. J. Kim, D. Yang, Z. Xie, J. Liu, Y. Xia, *ACS Nano,* 2011, **5**, 8212.
27 L. Wang, Y. Yamauchi, *J. Am. Chem. Soc.,* 2013, **135**, 16762.
28 P. J. Straney, L. E. Marbella, C. M. Andolina, N. T. Nuhfer, *J. Am. Chem. Soc.,* 2014, **136**, 7873.
29 F. -R. Fan, D. -Y. Liu, Y. -F. Wu, S. Duan, Z. -X. Xie, Z. -Y. Jiang, Z. -Q. Tian, *J. Am. Chem. Soc.,* 2013, **130**, 6949.
30 S. Xie, H-C. Peng, N. Lu, J. Wang, M. J. Kim, Z. Xie, Y. Xia, *J. Am. Chem. Soc.,* 2013, **135**, 16658.
31 W. Hong, J. Wang, E. Wang, *Appl. Mater. Interfaces,* 2014, **6**, 9481.
32 S. Xie, N. Lu, Z. Xie, J. Wang, M, J. Kim, Y. Xia, *Angew. Chem. Int. Ed.,* 2012, **51**, 10266.
33 C. Chen, Y. Kang, Z. Huo, Z. Zhu, W. Huang, H. L. Xin, J. D. Snyder, D. Li, J. A. Herron, M. Mavrikakis, M. Chi, K. L. More, Y. Li, N. M. Markovic, G. A. Somorjai, P. Yang, V. R. Stamenkovic, *Science,* 2014, **343**, 1339.